


Crossover between Athermal Jamming and the Thermal Glass Transition of Suspensions

M. Dinkgreve,¹ M. A. J. Michels,² T. G. Mason,³ and D. Bonn¹

¹*Institute of Physics, University of Amsterdam, Science Park 904, 1018 XH Amsterdam, Netherlands*

²*Department of Applied Physics, Eindhoven University of Technology, P.O. Box 513, 5600 MB Eindhoven, Netherlands*

³*Departments of Physics and Astronomy and Chemistry and Biochemistry, University of California, Los Angeles, California 90095, USA*

 (Received 25 January 2018; published 28 November 2018)

The non-Newtonian flow behavior of thermal and athermal disordered systems of dispersed uniform particles at high densities have strikingly similar features. By investigating the flow curves of yield-stress fluids and colloidal glasses having different volume fractions, particle sizes, and interactions, we show that both thermal and athermal systems exhibit power-law scaling with respect to the glass and jamming point, respectively, with the same exponents. All yield-stress flow curves can be scaled onto a single universal curve using the Laplace pressure as the stress scale for athermal systems and the osmotic pressure for the thermal systems. Strikingly, the details of interparticle interactions do not matter for the rescaling, showing that they are akin to usual phase transitions of the same universality class. The rescaling allows us to predict the flow properties of these systems from the volume fraction and known material properties.

DOI: [10.1103/PhysRevLett.121.228001](https://doi.org/10.1103/PhysRevLett.121.228001)

The transition between solidlike and liquidlike behavior in yield-stress fluids is a well-known phenomenon [1,2], that has remained poorly understood quantitatively [3,4]. An important established, but ill-understood, fact is that thermal and athermal systems share important similarities at the rheological level [5]. As an example, Fig. 1 shows the systems and the flow curves of a suspension of colloidal hard spheres [panels (a) and (c)] and of an athermal oil-in-water emulsion [panels (b) and (d)] at different volume fractions ϕ of particles and droplets. Both have a critical volume fraction ϕ_c above which a yield stress emerges, i.e., a concentration above which the amorphous solid behaves elastically for small deformations but flows when a stress is applied that exceeds the yield stress. Below ϕ_c , the material is a fluid having a viscosity that increases rapidly with ϕ . The hard-sphere thermal system undergoes a glass transition $\phi_c = \phi_G \sim 0.58$, while the purely athermal system exhibits a jamming transition $\phi_c = \phi_J \sim 0.64$, which corresponds to the maximum volume fraction of randomly packed solid objects (random close packing, rcp). The flow properties of both types of systems are often well described by the Herschel-Bulkley equation $\sigma = \sigma_y + K\dot{\gamma}^\beta$ (above ϕ_c) and the Cross equation $\sigma = \eta_N\dot{\gamma}/(1 + C\dot{\gamma}^{1-\delta})$ (below ϕ_c). Here, σ is the shear stress, σ_y is the yield (shear) stress, $\dot{\gamma}$ is the shear rate, η_N is the Newtonian viscosity and K , β , C , and δ are adjustable parameters. For athermal systems, the jamming transition is often characterized by a power-law dependence of the yield stress and the crossover rate to shear thinning on the distance to ϕ_c : $\sigma_y = \sigma_0|\Delta\phi|^\Delta$ and $\dot{\gamma}_{co} = \dot{\gamma}_0|\Delta\phi|^\Gamma$, with $|\Delta\phi| = |\phi - \phi_c|$, which then lead to a collapse of all concentration-dependent flow curves onto one supercritical and one subcritical branch [6–9].

The scalings with the distance to jamming and the subsequent collapse of the data are reminiscent of classical phase transitions. The central question we ask here is whether the jamming and glass transitions can both be understood in this way. There has been a lot of discussion in the literature about the analogy between jamming and critical phenomena. In theoretical treatments of jamming,

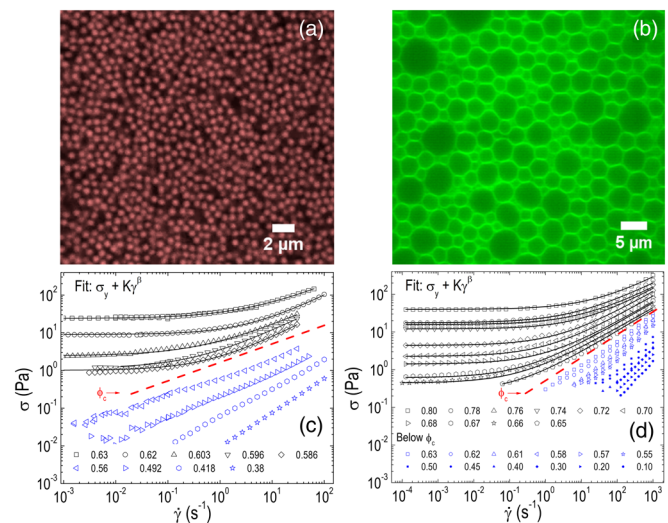


FIG. 1. Confocal microscope images and flow curves across the thermal colloidal glass transition for a suspension of PMMA hard spheres of radius $R \approx 183$ nm [10] (a) and (c) and an oil-in-water emulsion with droplet radius $R \approx 1.6$ μm across the athermal jamming transition [8] (b) and (d). In both cases, a yield stress appears above a certain critical density ϕ_c (dashed line). The black lines are fits to the Herschel-Bulkley model above ϕ_c .

the scaling exponents for athermal systems depend on the details of the interactions between particles [11–15], which excludes a universal treatment of different types of systems. On the other hand, experiments on athermal systems suggest that the collapse is rather universal [9]; also, a comparison of soft and hard particles, indeed, suggests that their rheology is similar, only with different stress scales that reflect the different interactions [16]. Simulations [17,18] suggest that the crossover between the jamming and the glass transition can also be described by assuming an additive combination of the different stresses from glass and jamming physics, $\sigma(\dot{\gamma}) = \sigma_G + \sigma_J + \eta_s \dot{\gamma}$. Therefore, the important question remains whether a universal rescaling of flow curves for thermal and athermal systems exists by an appropriate scaling of the stress scales.

Here, we investigate the crossover between thermal and athermal yield-stress regimes by comparing the flow curves of a variety of systems. First, we show that the flow curves of three different athermal emulsions with different inter-particle interactions can be collapsed with respect to the jamming transition, using the Laplace pressure as stress scale, and a common set of exponent values. Second, we study the flow curves of thermal systems; it is shown that they can be scaled in a way similar to the athermal systems and with very similar common exponent values. However, the rescaling now happens with respect to the glass transition and with the osmotic pressure as the stress scale. Finally, we demonstrate that all yield-stress flow curves of both thermal and athermal systems, over the full concentration range of the glass and jamming regimes, can be collapsed onto a single master curve taking the different contributions to the stress as additive. A simple microscopic two-state model of a balance between caged and flowing particles allows us to describe both regimes in these flow curves, pinpointing the origin of the observed universality. These results allow us to predict flow behavior merely from the constituent materials and their volume fractions, which was hitherto impossible, but has far-reaching implications.

The distinction between thermal and athermal systems is clear from the emergence of the yield stress: this happens at $\phi \approx 0.58$ for the glassy systems, and at $\phi \approx 0.64$ for the jamming systems. For athermal jamming, the characteristic stress and time scales originate from the interaction energy (ϵ) of the particles. We consider elastic emulsions that have a repulsive interaction energy which is due to the deformation of the droplets. The athermal emulsions interact through a screened Coulomb interaction, which becomes shorter ranged when more salt is added to the continuous phase. Therefore, the energy scale is set by the surface tension, and the stress scale is given by the Laplace pressure

$$\sigma_0 = \frac{\epsilon(R)}{R^3} = \frac{\Sigma}{R}, \quad (1)$$

with Σ the surface tension and R the particle radius. The corresponding time scale is

$$\tau_0 = \frac{\eta_0}{\sigma_0} = \frac{\eta_0 R}{\Sigma}, \quad (2)$$

with η_0 of the order of the solvent viscosity. Likewise, we can define the stress and time scales for Brownian motion with the thermal energy $k_B T$

$$\sigma_T = \frac{k_B T}{R^3}, \quad (3)$$

$$\tau_T = \frac{\eta_0}{\sigma_T} = \frac{\eta_0 R^3}{k_B T}. \quad (4)$$

From the above expressions, it becomes clear that the thermal and mechanical stresses are comparable when $k_B T \approx \epsilon$, while they become increasingly separated in the athermal limit $k_B T \ll \epsilon$ [18].

For the experiments, three types of athermal emulsions were prepared: castor oil-in-water emulsions with droplets of diameter $\sim 3.2 \mu\text{m}$ and a polydispersity of 10% (measured from confocal images). The use of different surfactants allows us to change the interactions [9,19]: 1 wt% sodium dodecyl sulphate in water (creating mobile surfaces), 0.4 wt% bovine serum albumin and 0.4 wt% propylene glycerol alginate (creating rigid surfaces), and 1 wt% sodium dodecyl sulphate in 0.05M NaCl (creating a screened and, hence, softer electrostatic interaction). The oil-water interfacial tension was measured for the three types of emulsions using a pendant-drop method [20]. Rheological measurements were performed on an Anton Paar MCR 302 using a roughened cone-plate geometry. The thermal systems are charge-stabilized, monodisperse silicone oil-in-water emulsions (having radii of 250, 530, and 740 nm) [21] and a poly (methyl methacrylate) (PMMA) colloidal glass (of radius 183 nm) [10]. An overview of the values for the surface tension, radius, and $\epsilon/k_B T$ for the different systems is given in the Supplemental Material [22].

First, we study the steady-state rheology of three different athermal emulsions; their flow curves are plotted in Fig. 2(a). The flow curves can then be collapsed onto master curves for the supercritical and subcritical data, with the critical volume fraction chosen as $\phi_J = 0.64$ (rcp). Determining the precise volume fraction for our emulsions is not a problem since we know exactly the volume fractions of water and oil when preparing the samples; this is more difficult for colloidal hard spheres [23]. However, for the rescalings presented below, the critical volume fractions ϕ_J and ϕ_G are independently determined experimentally by extrapolating where the yield stress goes to zero. The elasticity of the droplets and their deformation under compression is controlled by the Laplace pressure, Eq. (1). By plotting $\sigma/\sigma_0|\Delta\phi_J|^\Delta$ versus

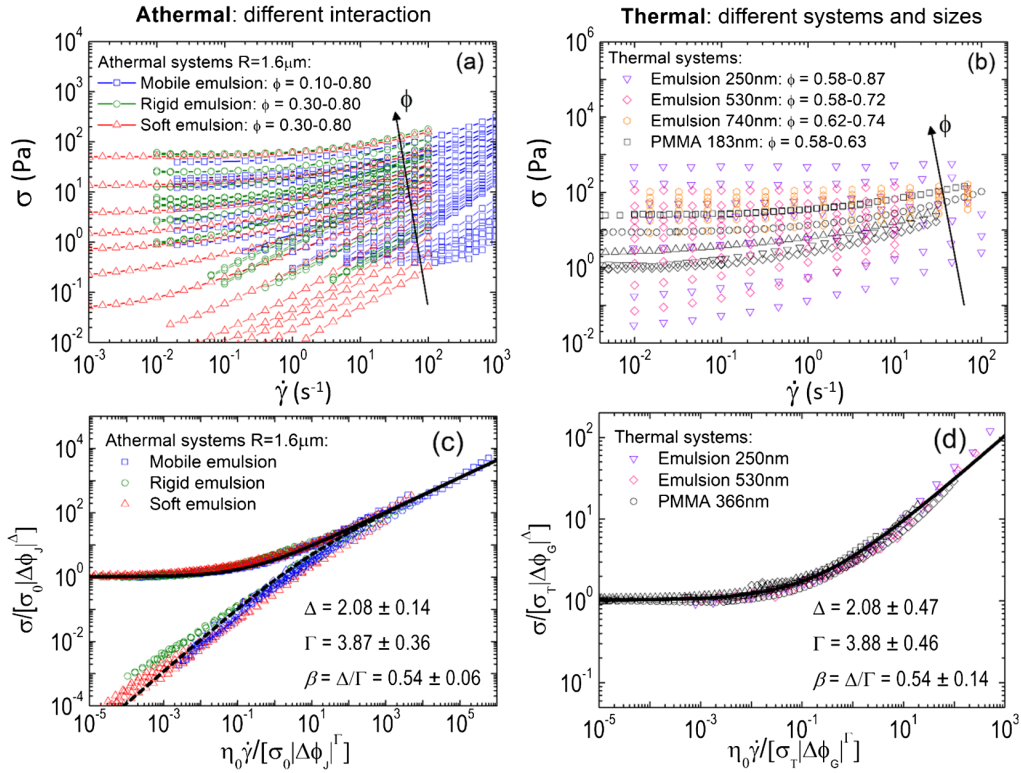


FIG. 2. (a) Flow curves of athermal castor oil-in-water emulsions with different interactions and different volume fractions ϕ . (b) Flow curves of thermal systems: different droplet sizes of silicone oil-in-water emulsions and PMMA particles. Volume fraction ϕ increases along the direction of the arrows, the exact values are listed in the Supplemental Material [22]. (c) Rescaled flow curves for athermal emulsions. The solid and dotted black lines are fits to the Herschel-Bulkley and Cross equations, respectively. (d) Rescaled flow curves for thermal systems below ϕ_J . The flow curves of the emulsion with $R = 740$ nm are not included here because they are not purely thermal; see Supplemental Material [22] for the result with the 740-nm emulsion included.

$\eta_0 \dot{\gamma} / \sigma_0 |\Delta \phi_J|^\Gamma$, with $\eta_0 = 1 \text{ mPas}$, all flow curves of the athermal emulsions can be collapsed onto a single curve [Fig. 2(c)]. For each flow curve of the different systems and volume fractions, the exponents Δ and Γ are adjusted, but their values remain in a narrow range: $\Delta = 2.08 \pm 0.14$ and $\Gamma = 3.87 \pm 0.36$. Using the same exponents, the subcritical flow curves (corresponding to fractions below ϕ_J) collapse automatically onto another master curve. The supercritical master curve can be fit to the Herschel-Bulkley equation $\sigma^* = 1.0 + 2.5 \dot{\gamma}^{*0.54}$, and the subcritical branch can be fitted to the Cross equation $\sigma^* = 1.2 \dot{\gamma}^* / (1 + 0.48 \dot{\gamma}^{*1-0.54})$, where σ^* and $\dot{\gamma}^*$ are dimensionless rescaled shear stress and shear rate, respectively.

For the thermal monodisperse emulsions [21] and PMMA hard-sphere colloidal glass [10] [Fig. 2(c)], the main difference with the case of athermal systems is that the glass transition can be observed to occur around $\phi_G \approx 0.58$. This is where the glass transition occurs for hard spheres, and the observation that thermal emulsions and colloidal hard-spheres show very similar behavior also indicates that this transition is independent of the interactions between the particles. We find that all flow curves can be collapsed if we scale them with respect to the glass transition and using the stress scale given by thermal fluctuations $k_B T / R^3$

[Fig. 2(d)]. To obtain this master curve, we find values for Δ and Γ that are strikingly similar to those found for the athermal flow curves, $\Delta = 2.08 \pm 0.47$ and $\Gamma = 3.88 \pm 0.46$. The stress scale is found to be proportional to the thermal stress $\sigma_T = \alpha k_B T / R^3$ with $\alpha = 35000$. The large prefactor α likely has to be attributed to the high entropic osmotic pressure that results from limited free volume for thermal motion [21,24,25]. A prefactor of order 10^4 can be calculated, e.g., from published MCT data for the thermal yield stress ($\phi = 0.60$, $\epsilon / k_B T = 10^5 - 10^7$), while simulations in this case give $\alpha \sim 10^3$ [26].

The flow curves of the thermal systems below ϕ_J shown above are dominated by the osmotic pressure. Ikeda *et al.* [17] show that, if the jamming and glass transitions are sufficiently separated, a new Newtonian regime of diverging viscosity should develop at high rates, controlled by the elastic interaction of the particles; above ϕ_J , a corresponding jamming yield stress appears. The latter high yield stress is obvious in the data of Fig. 2(b) for $\phi > \phi_J$, but a new Newtonian regime cannot be recognized for $\phi < \phi_J$. It appears that the two transitions are still insufficiently separated. We do note (i) that our thermal systems above ϕ_J and athermal systems show very similar jamming behavior, and (ii) that the glassy behavior of the thermal

systems is remarkably similar to the jamming behavior. The striking similarity of the glass and jamming yield point can be understood in terms of particle cage escape across a microscopic stress barrier, as described by a simple microscopic model for the critical transition (see Supplemental Material [22] and [9]).

As suggested by Ikeda *et al.* and borne out by our model, an additive combination of the characteristic stresses and rates enables us to superimpose all thermal and athermal flow curves, by plotting $\sigma/[\sigma_T|\Delta\phi_G|^\Delta + \theta\sigma_0|\Delta\phi_J|^\Delta]$ versus $\eta_0\dot{\gamma}/[\sigma_T|\Delta\phi_G|^\Gamma + \theta\sigma_0|\Delta\phi_J|^\Gamma]$ (Fig. 3). Here, we only needed to introduce, in view of the absent second Newtonian regime, a step function $\theta = 0$ if $\phi < \phi_J$ and $R < 1 \mu\text{m}$, and unity, otherwise, see Supplemental Material [22]. The striking conclusion is that, in this way, all flow curves, both thermal and athermal, collapse onto a single master curve with values of the exponents in a narrow range: $\Delta = 2.08 \pm 0.28$ and $\Gamma = 3.87 \pm 0.40$ (Fig. 4). Whether the exponents are truly universal or not is hard to judge and remains open to further investigation. There appears, e.g., a slight trend with particle size in the averages of the thermal systems, but data are limited and for fixed size there are sometimes large spreads in exponent values, pointing to numerical inaccuracy [see Supplemental Material [22], Fig. S2(a)]; note, also, that through the method of data collapse, any error in σ_y , σ_0 , or ϕ has been ignored and translated into an artificial error in Δ . In any case, these results imply that it is possible to predict the yield stress and flow behavior using only the volume fraction, particle sizes, and surface tension in a universal fashion.

We have shown that the flow curves of thermal and athermal systems can be scaled onto one universal curve using the Laplace pressure as stress scale for athermal systems and the osmotic pressure for the thermal systems, finding the same power-law exponents for the glass and jamming effects. For thermal systems, we have both hard-sphere colloids and thermal emulsions. In [27], it is

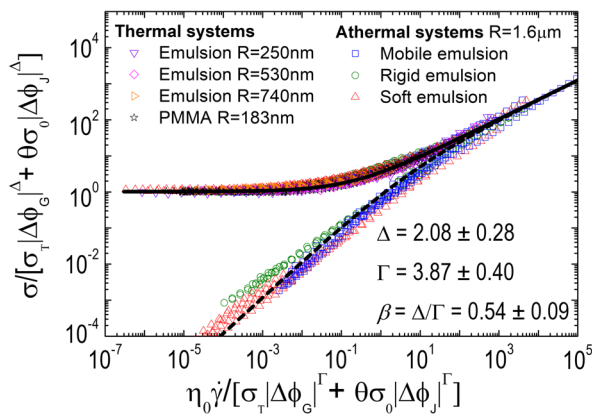


FIG. 3. Collapse of all thermal and athermal flow curves, with $\Delta = 2.08$ and $\Gamma = 3.87$. The solid and dotted black lines are fits to the Herschel-Bulkley and Cross equations, respectively.

proposed, for thermal systems, that the effective interaction of the analogous athermal system is a logarithmic repulsion, due to the entropic forces. This is valid for hard spheres very close to the jamming transition. Away from jamming, the validity of this mapping breaks down, and the interaction becomes of many-body type [28]. So the conclusion from our experiments is that, for the rescaling, it does not matter whether the spheres are hard or soft when they are thermal.

The athermal emulsions behave the same as the thermal systems, in the sense that their rescaling exponents are very similar. These are soft spheres with a harmonic interaction. There is no scaling for athermal hard spheres, because this case is a singular one: below ϕ_J , there is no yield stress, and at ϕ_J , there is, but it is impossible to go beyond ϕ_J for hard spheres because they cannot be compacted beyond random close packing [29]. In addition, Hertzian contact interactions between particles also give the exponents we find here [7]; in [16], it was shown that the interactions between these particles are best described by a Hertz contact.

As far as theory and simulations are concerned, for athermal systems, [30] shows why the rescaling exponents from simulations [13] are different from the experiments: the simulations probe a different regime much closer to jamming than can be achieved experimentally. A complete overview of all the different exponents and their possible relation with the interactions is given in [9]; specifically, the exponents that differ for different interactions are in the regime very close to jamming once again.

For the experiments, an additive combination of glass and jamming stresses is sufficient to achieve rescaling of all flow curves. The extension from jamming to the glass transition is easy to do within the simple microscopic model some of us introduced earlier (see [8,9] and Supplemental Material [22]) describing the heterogeneous dynamics in the system. The model considers that the fraction s of stagnant caged particles satisfies a balance equation and, thereby, becomes a function of the distance to the yield-stress line, independent of whether the system is thermal or athermal. The macroscopic flow-rate

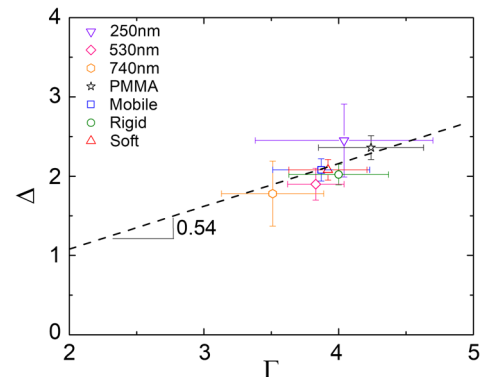


FIG. 4. Δ versus Γ for the different thermal and athermal systems with corresponding standard deviations.

dependence of the stress then follows from the microscopic rate of stress-induced cage escape and its relation to a length scale of cooperative motion. This heterogeneity length scale diverges as a power-law in $|s - s_c|$ when approaching the critical yield stress, implying that we consider a second-order dynamical critical transition. This microscopic two-state picture of a balance between caged and flowing particles can, therefore, be applied both to the jamming and the glass transition. This is again reminiscent of classical phase transitions, where the fluctuations dominate the interactions, resulting in a universal behavior.

In conclusion, we propose a scaling that applies to both thermal and athermal systems, finding universal exponents for the jamming and glass transitions. This means that we can predict, rather than fit, characteristic stress and rate prefactors from material properties and, hence, predict flow properties. This is of considerable importance for, e.g., the food or oil industries; once the volume fractions, drop sizes, and interfacial tensions are known, an accurate estimate of the yield stress and post-yield viscosity can be made that will allow us to tailor food properties or help to improve oil recovery rates.

We thank G. Petekidis for sending his rheology data used in this work.

-
- [1] R. G. Larson, *The Structure and Rheology of Complex Fluids* (Oxford University Press, New York, 1999).
 - [2] P. Coussot, *Rheometry of Pastes, Suspensions, and Granular Materials: Applications in Industry and Environment* (John Wiley and Sons, New York, 2005).
 - [3] L. Berthier and G. Biroli, *Rev. Mod. Phys.* **83**, 587 (2011).
 - [4] A. J. Liu and S. R. Nagel, *Annu. Rev. Condens. Matter Phys.* **1**, 347 (2010).
 - [5] D. Bonn, M. M. Denn, L. Berthier, T. Divoux, and S. Manneville, *Rev. Mod. Phys.* **89**, 035005 (2017).
 - [6] P. Olsson and S. Teitel, *Phys. Rev. Lett.* **99**, 178001 (2007).
 - [7] K. N. Nordstrom, E. Verneuil, P. E. Arratia, A. Basu, Z. Zhang, A. G. Yodh, J. P. Gollub, and D. J. Durian, *Phys. Rev. Lett.* **105**, 175701 (2010).
 - [8] J. Paredes, M. A. J. Michels, and D. Bonn, *Phys. Rev. Lett.* **111**, 015701 (2013).

- [9] M. Dinkgreve, J. Paredes, M. A. J. Michels, and D. Bonn, *Phys. Rev. E* **92**, 012305 (2015).
- [10] G. Petekidis, D. Vlassopoulos, and P. N. Pusey, *J. Phys. Condens. Matter* **16**, S3955 (2004).
- [11] C. S. O'Hern, S. A. Langer, A. J. Liu, and S. R. Nagel, *Phys. Rev. Lett.* **88**, 075507 (2002).
- [12] C. S. O'Hern, L. E. Silbert, A. J. Liu, and S. R. Nagel, *Phys. Rev. E* **68**, 011306 (2003).
- [13] B. P. Tighe, E. Woldhuis, J. C. Remmers, W. van Saarloos, and M. van Hecke, *Phys. Rev. Lett.* **105**, 088303 (2010).
- [14] G. Katgert, B. P. Tighe, and M. van Hecke, *Soft Matter* **9**, 9739 (2013).
- [15] C. P. Goodrich, S. Dagois-Bohy, B. P. Tighe, M. van Hecke, A. J. Liu, and S. R. Nagel, *Phys. Rev. E* **90**, 022138 (2014).
- [16] K. van der Vaart, Y. Rahmani, R. Zargar, Z. Hu, D. Bonn, and P. Schall, *J. Rheol.* **57**, 1195 (2013).
- [17] A. Ikeda, L. Berthier, and P. Sollich, *Phys. Rev. Lett.* **109**, 018301 (2012).
- [18] A. Ikeda, L. Berthier, and P. Sollich, *Soft Matter* **9**, 7669 (2013).
- [19] S. A. Koehler, S. Hilgenfeldt, E. R. Weeks, and H. A. Stone, *Phys. Rev. E* **66**, 040601(R) (2002).
- [20] J. D. Berry, M. J. Neeson, R. R. Dagastine, D. Y. C. Chan, and R. F. Tabor, *J. Colloid Interface Sci.* **454**, 226 (2015).
- [21] T. G. Mason, J. Bibette, and D. A. Weitz, *J. Colloid Interface Sci.* **179**, 439 (1996).
- [22] See Supplemental Material at <http://link.aps.org/supplemental/10.1103/PhysRevLett.121.228001> for material properties, additional figures and details of the extended jamming model.
- [23] W. C. Poon, E. R. Weeks, and C. P. Royall, *Soft Matter* **8**, 21 (2012).
- [24] H. S. Kim, F. Scheffold, and T. G. Mason, *Rheol. Acta* **55**, 683 (2016).
- [25] M. Braibanti, H. S. Kim, N. Şenbil, M. J. Pagenkopp, T. G. Mason, and F. Scheffold, *Sci. Rep.* **7**, 13879 (2017).
- [26] A. Ikeda and L. Berthier, *Phys. Rev. E* **88**, 052305 (2013).
- [27] M. Trulsson, M. Bouzid, J. Kurchan, E. Clément, P. Claudin, and B. Andreotti, *Europhys. Lett.* **111**, 18001 (2015).
- [28] G. Parisi, Y. G. Pollack, I. Procaccia, C. Rainone, and M. Singh, *Phys. Rev. E* **97**, 063003 (2018).
- [29] M. Wyart, *Ann. Phys. Fr.* **30**, 1 (2005).
- [30] R. I. Dekker, M. Dinkgreve, H. de Cagny, D. Koeze, B. Tighe, and D. Bonn, *J. Non-Newtonian Fluid Mech.* **261**, 33 (2018).